Title

Determination of the Number of Tube Rows to Obtain Closure for Volume Averaging Theory Based Model of Fin-and-Tube Heat Exchangers

Journal

Journal of Heat Transfer, 133(12)

ISSN

00221481

Authors

Zhou, Feng
Hansen, Nicholas E
Geb, David J
et al.

Publication Date

2011

DOI

10.1115/1.4004478

Peer reviewed

Determination of the Number of Tube Rows to Obtain Closure for Volume Averaging Theory Based Model of Fin-and-Tube Heat Exchangers

Feng Zhou
School of Energy and Environment,
Southeast University,
2 Si Pai Lou, Nanjing 210096, China;
Department of Mechanical and Aerospace Engineering,
University of California,
48-121 Engineering IV, 420 Westwood Plaza,
Los Angeles, CA 90095
e-mail: zhoufeng@ucla.edu

Nicholas E. Hansen
e-mail: hansenen@gmail.com

David J. Geb
e-mail: dvdgb18@yahoo.com

Ivan Catton
e-mail: catton@ucla.edu

Department of Mechanical and Aerospace Engineering,
University of California,
48–121 Engineering IV, 420 Westwood Plaza,
Los Angeles, CA 90095

Modeling of fin-and-tube heat exchangers based on the volume averaging theory (VAT) requires proper closure of the VAT based governing equations. Closure can be obtained from reasonable lower scale solutions of a computational fluid dynamics (CFD) code, which means the tube row number chosen should be large enough, so that the closure can be evaluated for a representative elementary volume (REV) that is, not affected by the entrance or recirculation at the outlet of the fin gap. To determine the number of tube rows, three-dimensional numerical simulations for plate fin-and-tube heat exchangers were performed, with the Reynolds number varying from 500 to 6000 and the number of tube rows varying from 1 to 9. A clear perspective of the variations of both overall and local fiction factor and the Nusselt number as the tube row number increases are presented. These variation trends are explained from the view point of the field synergy principle (FSP). Our investigation shows that $4+1+1$ tube rows is the minimum number to get reasonable lower scale solutions. A computational domain including $5+2+2$ tube rows is recommended, so that the closure formulas for drag resistance coefficient and heat transfer coefficient could be evaluated for the sixth and seventh elementary volumes to close the VAT based model. [DOI: 10.1115/1.4004478]

Keywords: volume averaging theory, closure, field synergy principle, fin-and-tube heat exchanger, representative elementary volume

Introduction

Volume averaging theory (VAT) is an approach that can be applied to many different types of transport phenomena [1–7] and has been used to rigorously cast the point-wise conservation of energy, momentum and mass equations into a form that represents the thermal and hydraulic properties of fin-and-tube heat exchanger morphology. Using the VAT to optimize the flow and heat transfer in heat exchangers, a more general model that can easily be adapted to many different structures can be made. By modeling heat exchangers as porous media, specific geometry can be accounted for in such a way that the details of the original structure can be replaced by their averaged counterparts and the governing VAT equations can be solved for a wide range of heat exchanger designs. The tricky part about using VAT is that proper closure is needed to complete the governing equations. Closure for both the VAT based momentum and energy equations have been strictly deduced and defined by Travkin and Catton [3], making it possible to use lower scale flow and temperature fields to obtain closure for VAT based governing equations of heat exchangers.

The closure formula for momentum equation is a drag coefficient represented by

$$c_d = 2\frac{\int_{\partial S_w}\tilde{p}\cdot d\vec{s}}{\rho_f\tilde{\tilde{u}}^2 A_{wp}}\frac{S_{wp}}{S_w} + 2\frac{\int_{\partial S_w}\tau_{wL}\cdot d\vec{s}}{\rho_f\tilde{\tilde{u}}^2 A_w} + 2\frac{\int_{\partial S_w}\tau_{wT}\cdot d\vec{s}}{\rho_f\tilde{\tilde{u}}^2 A_w} - \frac{\frac{\partial}{\partial x_j}\langle\hat{\tilde{u}}_i\hat{\tilde{u}}_j\rangle_f}{\frac{1}{2}\rho\tilde{\tilde{u}}^2} + \frac{\frac{\partial}{\partial x_j}\left(\left\langle \nu_T\frac{\partial\tilde{\tilde{u}}_i}{\partial x_j}\right\rangle_f\right)}{\frac{1}{2}\rho\tilde{\tilde{u}}^2} \tag{1}$$

The closure formula for energy equation is the heat transfer between phases given by

$$h = \frac{\frac{1}{\Delta\Omega}\int_{\partial S_w}(k_f+k_T)\nabla T_f\cdot d\vec{s}}{S_w(\tilde{T}_s-\tilde{T}_f)} - \frac{\rho_f c_{pf}\nabla\cdot\left(\langle m\rangle\widetilde{\hat{u}_f\hat{T}_f}\right)}{S_w(\tilde{T}_s-\tilde{T}_f)} + \frac{\nabla\cdot\left(\frac{k_f}{\Delta\Omega}\int_{\partial S_w}T_f d\vec{s}\right)}{S_w(\tilde{T}_s-\tilde{T}_f)} \tag{2}$$

Closure can be obtained by applying Eqs. (1) and (2) on a selected representative elementary volume (REV) of particular heat exchanger morphology. To treat a fin-and-tube heat exchanger as porous media, entrance effects are important for both momentum and energy transport. When flow enters porous media, temperature and velocity profiles are uniform across the entrance area and as the flow progresses further downstream from the inlet, both thermal and momentum boundary layer are getting thicker until they merge with its counterpart at some particular location. Also, local values differ from the overall averaged as expected, therefore special attention should be paid when one uses the drag coefficient and heat transfer coefficient with the VAT governing equations to solve large scale problem. Local values are the only values that have a physical meaning when describing transport phenomena with the VAT macro scale equations. Therefore, before evaluating the friction factor c_d and heat transfer coefficient h from the output of a CFD code, the tube row number one needs to simulate to obtain reasonable lower scale solutions must be determined.

Extensive investigations on the performance of fin-and-tube heat exchanger have been done, either experimentally or numerically. Rich [8] presented the experimental results for six coils,

Contributed by the Heat Transfer Division of ASME for publication in the Journal of Heat Transfer. Manuscript received January 3, 2011; final manuscript received June 19, 2011; published online October 6, 2011. Assoc. Editor: Sujoy Kumar Saha.

with the number of tube rows in the direction of air flow varying from 1 to 6. It was concluded that the pressure drop per row is independent of the number of tube rows. McQuiston [9] proposed the first well-known correlation for plate fin-and-tube heat exchangers with tube row number being in the range of 1–4. Based on a superposition model which was initially proposed by Rich [10], Gray and Webb [11] gave an updated correlation for fin-and-tube heat exchangers that is superior to McQuiston's [9]. It should be noted that the correlations were based on the experimental data for 4-row fin-and-tube heat exchangers. Kang et al. [12] presented experimental data and correlations for a 3-row fin-and-tube heat exchanger core in a wide range of the Reynolds number. Most recently, Wang et al. [13] proposed what is at this time the most precise correlations for the friction factor and heat transfer coefficient on the air side of fin-and-tube heat exchangers. The correlations are based on a total of 74 samples and the proposed heat transfer correlation can describe 88.6% of the database within ±15%, while the proposed friction correlation can correlate 85.1% of the database within ± 15%. However, it is applicable only for up to six tube rows. Besides experimental investigations, many numerical simulations of plate fin-and-tube heat exchangers were reported. Torikoshi et al. [14] reported simulation results for 1-row and 2-row fin-and-tube heat exchangers. Jang et al. [15–17] did extensive numerical and experimental studies on fluid flow and heat transfer over a multirow (1–6 rows) fin-and-tube heat exchanger. It was reported that the number of tube rows has a small effect on the average heat transfer coefficient when the row number was larger than 4.

After reviewing the literature, there are three problems we need to point out. The first is that most of the studies reviewed above were limited to small number of tube rows. This is not enough to determine how large the tube row number must be to simulate the process in order to get reasonable lower scale solutions. The second that should be noted is that most of these investigations are based on the average parameters over the whole domain. While for VAT based modeling, only the local values can be used in calculations to accurately predict total heat transfer in porous media. Therefore, the influence of tube row number on local heat transfer characteristics needs to be clearly revealed. The third problem is related to the air side recirculation between the fin-and-tube region and the extended region. The elementary volumes being affected by the recirculation should not be used to calculate the closure for the VAT based model. The above three issues are the motivation of the present study.

In the current paper, 3D numerical simulations for plate fin-and-tube heat exchangers were performed, with the Reynolds number varying from 500 to 6000 and tube row number varying from 1 to 9. A clear perspective of the variations of both overall and local fiction factor and Nusselt number as the tube row number increases was presented. These variation trends are also explained from the view point of field synergy principle, a novel concept proposed and verified by Guo and some other researchers [18–22]. The basic mechanism of FSP is that the convective heat transfer could be enhanced by decreasing the intersection angle between the velocity and the temperature gradient. The changing tendency of this intersection angle, in turn, provides a helpful means to explain the variation in trends of the heat transfer coefficient and could help to further verify the tube row number one should simulate to get reasonable lower scale solutions for the VAT based modeling. Considering that both the traditional analysis method and the novel FSP analysis came to the same conclusion, a specific tube row number is proposed.

Physical Model and Numerical Method

Physical Model. A schematic diagram of a plate fin-and-tube heat exchanger is shown in Fig. 1. There usually three or more rows of tubes which are arranged in-line or staggered. The dimensions of the main geometrical parameters, like tube diameter (D_i, D_o, and D_c), tube transverse pitch (P_t), tube longitudinal pitch (P_l), fin pitch (F_p), and fin thickness (δ_f) are tabulated in Table 1, which are the same as those of the sample core tested by Kang et al. [12] experimentally.

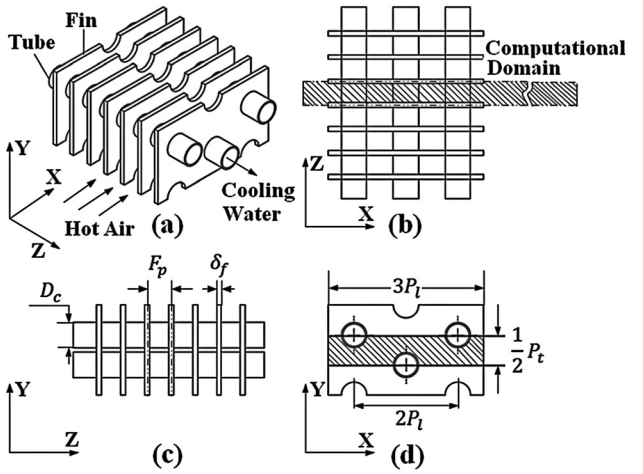

Fig. 1 A schematic diagram of a plain plate fin-and-tube heat exchanger

Here we consider the hot air flow across the fin side, while the cooling water flows through the tubes. The tubes and fins are constructed of copper and aluminum, respectively. Both fluids are assumed to be incompressible with constant properties. Due to the relatively large heat transfer coefficient on the tube side, the tube inner wall temperature was set equal to the fluid temperature. The conjugate effect of the tube wall was treated enabling the fin effect to be properly incorporated into the problem [23].

Flow Model and Governing Equations. In this study, laminar steady model is adopted for the flow within the Reynolds number range of 500–6000. The choice of flow model is explained as follows. First, if the flow between two adjacent fins is considered as channel flow, the transition Reynolds number is around 2300, with the double fin spacing as the reference length for Re. In this study, the fin collar diameter is 10.55mm, which is about 5.3 times of the fin spacing, thus the transition Reynolds number of 2300 corresponds to around 6066 based on the fin collar diameter. If the flow between two adjacent fins is regarded as the flow past a cylinder, the turbulent flow occurs when the Reynolds number is over 1.4×10^5 [24]. Second, although flow visualization shows that when the Reynolds number is over 100, unsteady wake occurs behind the cylinder, from engineering point of view, we care more about the averaged parameters, like averaged friction factor and the Nusselt number. Third, many studies, which adopted steady and laminar model for flow and heat transfer analysis of fin-and-tube heat exchangers, obtained reasonably good results and have been published in international journals [15–17,25,26]. Finally, to further verify the laminar assumption, both laminar model and SST model were adopted to calculate the case for Reynolds number of 6000, the difference turned out to be negligible.

Table 1 Some data of the fin-and-tube heat exchanger

Tube row arrangement	Staggered
Tube material	Copper
Fin material	Aluminium
Tube inner diameter, D_i	9.33 mm
Tube outer diameter, D_o	10.15 mm
Fin collar diameter, D_c	10.55 mm
Tube transverse pitch, P_t	25 mm
Tube longitudinal pitch, P_l	21.65 mm
Fin thickness, δ_f	0.2 mm
Fin pitch, F_p	2.2 mm

The governing equations for continuity, momentum and energy in the computational domain can be expressed as follows:

Continuity equation

$$\frac{\partial u_i}{\partial x_i} = 0 \tag{3}$$

Momentum equation

$$\frac{\partial}{\partial x_i}(u_i u_k) = \frac{\mu}{\rho}\frac{\partial}{\partial x_i}\left(\frac{\partial u_k}{\partial x_i}\right) - \frac{1}{\rho}\frac{\partial p}{\partial x_k} \tag{4}$$

Energy equation

$$\frac{\partial}{\partial x_i}(u_i T) = \frac{k}{\rho c_p}\frac{\partial}{\partial x_i}\left(\frac{\partial T}{\partial x_i}\right) \tag{5}$$

The boundary conditions assigned for the computational domain are tabulated in Table 2.

SC/Tetra HPC Solver was used to solve the governing equations. The numerical techniques and discretization schemes used in the code are a 2nd order Monotone Upstream-centered Schemes for Conservation Laws for convective terms in the energy and momentum equations while for the momentum and energy diffusion terms, an accuracy weighted scheme is used. A corrected version of the Semi-Implicit Method of the Pressure Linked Equations (SIMPLEC) is used [23,27] for the pressure correction.

Computational Domain and Grid System. Since the fin-and-tube heat exchanger has symmetry and periodicity in the y and z directions, the cell between two adjacent fin surfaces is simulated with half of the fin thickness at the upper and the bottom sides, just as Figs. 1(b)–1(d) shows. The actual length of computation domain was 7.5 times the fin and tube region in the flow direction, see Fig. 2. Because of the thickness of the fin, the air velocity profile at the entrance is not uniform. The computational domain is then extended upstream 1.5 times the stream-wise fin length, so that a uniform velocity distribution can be ensured at the domain inlet. The computational domain is extended downstream 5 times the stream-wise fin length, so that at the outer flow boundary no flow recirculation exits and the local one-way method can be used for the numerical treatment of the outer flow boundary condition [27].

A commercial finite volume code SC/Tetra v8 (2009) is used to do the 3D CFD simulation. This code utilizes a vertex based scheme for which the discrete equations are written in a relatively simple form and the number of control volumes is reduced compared to cell centered formulation. The grid system for the configurations is built by SC/Tetra Pre, which controls the size of the mesh three dimensionally by creating an octree. When creating an octree, octants are refined automatically to prevent them from differing by two or more levels from the next octant. Mesh adaptive analysis was used to build the grid system. Fine elements are arranged where the change of pressure, velocity or temperature is large. As can be seen in Fig. 3, fine elements were successfully arranged where the flow shows important phenomena, such as the region behind the tubes, boundaries that cause large temperature and/or flow changes, etc. Coarse elements were assigned where

Table 2 Boundary conditions

Inlet	$u = \text{const}, v = w = 0, T = \text{const}$
Outlet	$\frac{\partial u_i}{\partial x} = \frac{\partial T}{\partial x} = 0$
Eight surfaces of the extended region	symmetric, slip, and adiabatic wall
Interface between air and solid	no-slip, no thermal resistance
Tube inside wall	$u = v = w = 0, T_w = \text{const}$
The other surfaces	symmetric

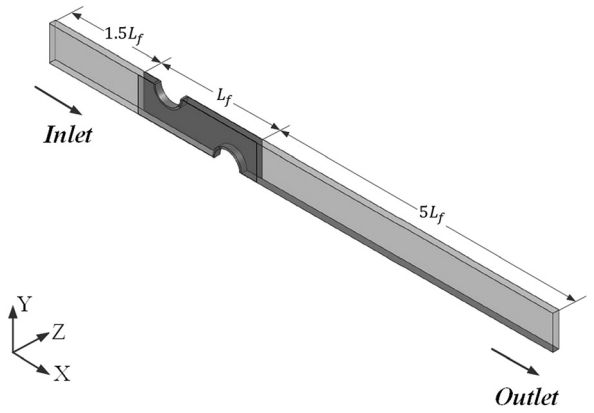

Fig. 2 Computational domain (It is not drawn to scale)

little change occurs, especially in the extended region. It can also be observed that the grid system has gradual variation from fine elements to coarse elements, which is quite important to maintain the calculation accuracy.

Grid independence tests were made carefully, and the numerical results obtained can be regarded as grid-independent. Take the two-row model as an example, where grid systems with 6,97,849, 1,728,574, 2,639,059, 3,860,677, 4,985,479, 6,607,223, and 8,177,712 elements were tested, and comparing the results of the finest grid with the second finest one, a 1.3% difference was yielded. To save computer resources but also get a reasonable accuracy, the sixth grid system was adopted. Table 3 shows the element numbers used for the nine cases of our computation.

Parameter Definitions

Definitions for the characteristic quantities which will be used in the analysis of numerical results are presented the following:

$$\text{Re} = \frac{\rho u_{\max} D_c}{\mu} \tag{6}$$

$$\text{Nu} = \frac{hD_c}{k} \tag{7}$$

$$h = \frac{\Phi}{A_o \Delta T \eta_o} \tag{8}$$

$$\Phi = \dot{m} c_p (T_{\text{in}} - T_{\text{out}}) \tag{9}$$

$$\Delta T = \frac{T_{\max} - T_{\min}}{\log(T_{\max}/T_{\min})} \tag{10}$$

$$\eta_o = 1 - \frac{A_f}{A_o}(1 - \eta_f) \tag{11}$$

$$A_f = N\left[P_t P_l - \pi\left(\frac{D_c}{2}\right)^2\right] \tag{12}$$

$$A_o = N\left[P_t P_l - \pi\left(\frac{D_c}{2}\right)^2 + \frac{1}{2}\pi D_c (F_p - \delta_f)\right] \tag{13}$$

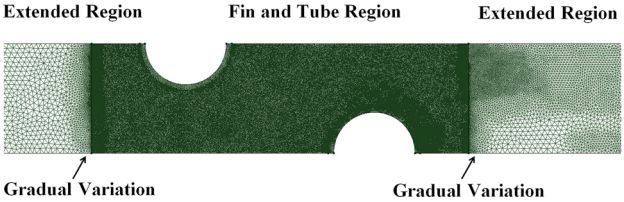

Fig. 3 Grid system for 2-row case

Table 3 Element number of each case

Row number	Elements	Row number	Elements
$N=1$	5,631,456	$N=6$	11,406,636
$N=2$	6,607,223	$N=7$	13,951,880
$N=3$	8,093,309	$N=8$	15,852,835
$N=4$	8,910,684	$N=9$	17,623,983
$N=5$	10,396,075	—	—

$$f = \frac{\Delta p}{\frac{1}{2}\rho u_{\max}^2} \cdot \frac{D_c}{L} \tag{14}$$

$$\Delta p = p_{\text{in}} - p_{\text{out}} \tag{15}$$

where $u_{\max}$ is the mean velocity at the minimum cross section, $T_{\max} = \max(T_{\text{in}} - T_w, T_{\text{out}} - T_w)$, $T_{\min} = \min(T_{\text{in}} - T_w, T_{\text{out}} - T_w)$, Φ is the actual heat transfer rate between air and the fin surface.

As has been discussed above, the computation is of a conjugated type where the fin efficiency is determined during the computations and cannot be obtained in advance. According to heat transfer theory [28,29], the fin efficiency is defined as the actual heat transfer rate from the fin and tube divided by the heat transfer rate from the fin and tube when the fin is at the same temperature as the tube. In our numerical simulations, the fin efficiency η_f is computed by the approximation method described by Schmidt [30] and is as follows:

$$\eta_f = \frac{\tanh(mr\phi)}{mr\phi} \tag{16}$$

where

$$m = \sqrt{\frac{2h}{k_f \delta_f}} \tag{17}$$

$$\phi = \left(\frac{R_{eq}}{r} - 1\right)\left[1 + 0.35ln\left(\frac{R_{eq}}{r}\right)\right] \tag{18}$$

For a staggered tube layout

$$\frac{R_{eq}}{r} = 1.27\frac{X_M}{r}\left(\frac{X_L}{X_M} - 0.3\right)^{1/2} \tag{19}$$

$$X_L = \frac{\sqrt{(P_t/2)^2 + P_l^2}}{2} \tag{20}$$

$$X_M = P_t/2 \tag{21}$$

For an inline tube layout, or a 1-row fin-and-tube heat exchanger

$$\frac{R_{eq}}{r} = 1.28\frac{X_M}{r}\left(\frac{X_L}{X_M} - 0.2\right)^{1/2} \tag{22}$$

$$X_L = P_l/2 \tag{23}$$

$$X_M = P_t/2 \tag{24}$$

To analyze the numerical results using the field synergy principle, the concept of FSP is briefly reviewed as follows.

For a steady-state elliptic flow of constant properties within an computational domain (taking the fluid flow and heat transfer over a backward step [31] as an example, as shown in Fig. 4), its energy conservation equation can be described as

$$\rho c_p\left(u\frac{\partial T}{\partial x} + v\frac{\partial T}{\partial y} + w\frac{\partial T}{\partial z}\right) = k_f\left(\frac{\partial^2 T}{\partial x^2} + \frac{\partial^2 T}{\partial y^2} + \frac{\partial^2 T}{\partial z^2}\right) \tag{25}$$

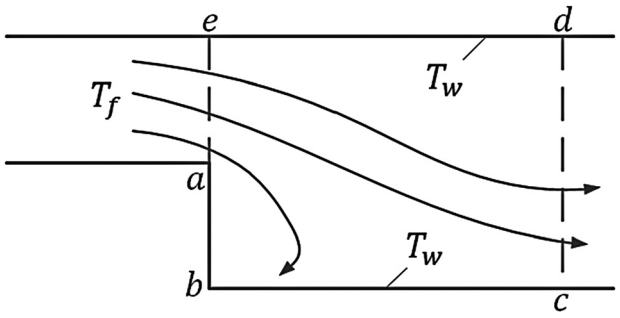

Fig. 4 Fluid flow and heat transfer over a backward step

Integrate Eq. (25) over the entire domain Ω_{abcde} leading to

$$\int_{\Omega_{abcde}} \rho c_p(\vec{U}\cdot\nabla T)dA = \int_{\Omega_{abcde}} k_f \nabla^2 T dA \tag{26}$$

Incorporating the Gauss law for reduction of the integral dimension, the right side of Eq. (26) can be written as

$$\int_{\Omega_{abcde}} k_f \nabla^2 T dA = \int_{abc} k_f \vec{n}\cdot\nabla T ds + \int_{de} k_f \vec{n}\cdot\nabla T ds + \int_{cd} k_f \vec{n}\cdot\nabla T ds + \int_{ea} k_f \vec{n}\cdot\nabla T ds \tag{27}$$

The last two terms on the right-hand side of Eq. (27) represent the axial heat conduction within the fluid while the first two terms stand for the convective heat transfer between the fluid and solid. For flow with Peclet number greater than 100, the axial conduction terms can be neglected [32], leading to

$$\int_{\Omega_{abcde}} \rho c_p(\vec{U}\cdot\nabla T)dA = \int_{abc} k_f \vec{n}\cdot\nabla T ds + \int_{de} k_f \vec{n}\cdot\nabla T ds \tag{28}$$

For conventional working fluids adopted in engineering, the Peclet numbers are usually greater than 100, and hence, the integration $\int_{\Omega_{abcde}} \rho c_p(\vec{U}\cdot\nabla T)dA$ actually represents the energy transferred by convection [31]. The inner production $\vec{U}\cdot\nabla T = |\vec{U}||\nabla T|\cos\theta$, in which θ is the local intersection angle between the local velocity vector and the temperature gradient. Therefore, it is obvious that besides increasing the velocity and temperature gradient, decreasing their intersection angle θ will also make the integration $\int_{\Omega_{abcde}} \rho c_p(\vec{U}\cdot\nabla T)dA$ larger, enhancing the heat transfer. On the other hand, for a given flow rate and temperature gradient, the changing tendency of this intersection angle helps explain the variation in trends of the convective heat transfer coefficient, which further verifies the tube row number one should simulate to get reasonable lower scale solutions for the VAT based modeling.

According to the concept of this principle, the following quantity is introduced

$$M = \frac{\sum(|\vec{U}||\nabla T|)}{n} \tag{29}$$

The local intersection angle between the velocity and temperature gradient is

$$\theta = cos^{-1}\frac{u\frac{\partial T}{\partial x} + v\frac{\delta T}{\delta y} + w\frac{\partial T}{\partial z}}{|\vec{U}||\nabla T|} \tag{30}$$

The average intersection angle of the computation domain is defined by

$$\theta_m = \frac{\sum_{i,j,k}^{\theta} dv_{i,j,k}}{\sum dv_{i,j,k}} \tag{31}$$

where $dv_{i,j,k}$ is the volume element of the control volume (i, j, k).

Numerical Results and Discussion

Validation of the CFD Code and the Simulation Method. To verify the computational model and the method adopted in numerical simulation, preliminary computations were first conducted for a 3-row plate fin-and-tube heat exchanger. The dimensions used in the simulation are the same as those of the heat exchanger measured by Kang et al. [12] for his experiments.

The Nusselt number and friction factor obtained from simulation solutions were compared with the correlations and experimental data by Kang et al. [12] and the correlations by Wang et al. [13] and are shown in Fig. 5. From Fig. 5 we can see that the maximum deviation of the friction factor and the Nusselt number from experiment are 10.4% and 11.9% with the average deviation being around 6% and 5.5%, respectively. Our predicted results and the experimental data agree very well, thereby showing the reliability of the physical model and the adopted numerical method.

Validation of FSP Application. To verify that the FSP is suitable to our problem, computation was conducted for the 3-row case and the effect of Reynolds number on heat transfer characteristic of plate fin-and-tube heat exchangers was analyzed by FSP. The Reynolds number based on the fin collar outside diameter varied from 500 to 6000 and the corresponding air frontal velocity was ranged from 0.38 m/s to 4.6 m/s.

Figure 6 shows the variation of M/M_0 as a function of the Reynolds number, where M_0 is the value of M when $\mathrm{Re} = 500$. In the Reynolds number range of our computation, the increase in air flow velocity is the main reason why the heat transfer rate increased. Therefore, it is not surprising that the value of M has a nearly linear-increasing relationship with the Reynolds number, which should lead the Nusselt number to be proportional to Re. However, the increasing trend of the average Nusselt number with Re was weakened as the Reynolds number increases, just as Fig. 7 shows. The reason why this happened is that the intersection angle between velocity and temperature gradient increased with Re, shown in Fig. 7, which leads to the worsening of the synergy. Consequently, the increasing trend of the intersection angle is similar to that of the Nusselt number.

Figures 8–10 present the local distributions of velocity (a), temperature (b) and intersection angle (c) on the x-y plane at $z = 0.0011$ m for $\mathrm{Re} = 500$, 3000 and 6000, respectively. Basically, these pictures reveal two main pieces of information:

(1) The synergy becomes worse in the direction of air flow stream. At the inlet region, the isothermals are almost perpendicular to the velocity vector, which leads to a quite small intersection angle at the inlet part. After the flow passes through the first tube, the velocity vector almost parallels the isothermals, which results in a worse synergy.
(2) That synergy becomes worse with increasing the Reynolds number can be observed qualitatively by noting region of red color in the paint graphs of intersection angle distribution. Comparing Fig. 10 with Fig. 8, we find that for large Reynolds number, even at the inlet, the synergy is not good, let alone the remaining part of the simulation region. Therefore, the increase of heat transfer rate brought by the increase of air flow velocity is counteracted partly by the deteriorated synergy.

Based on the above analysis, the increasing trend of Nusselt number with Reynolds number was explained well by the FSP. Thus, it is meaningful to use FSP to analyze the heat transfer characteristic of plate fin-and-tube heat exchangers and help to determine the tube row number for our purpose without any simplifying assumption, such as ideal fin and ideal temperature difference, which was adopted by studies [19–22] while verifying the FSP.

Determine the Length of Computational Domain. It should be noted that the number of tube rows has a different effects on the friction factor than the Nusselt number of fin-and-tube heat exchangers. Fig. 11, which was plotted using the correlations given by Wang et al. [13] illustrates the difference.

As can be seen in Fig. 11, for fin-and-tube heat exchangers with multiple-row tubes, the friction factors are almost independent of the number of tube rows, while the Nusselt number decreases with the increasing of tube row number. Our simulation results, conducted with the tube row number varying from 1 to 9, came to the same conclusion, shown by Fig. 12. It can be seen that the variation of friction factor with N is quite small, and when the row number is larger than 3, f could be considered independent of N. Wang et al. [33,34] also arrived at the same conclusion by means of experiments. It is also shown that the Nusselt number decreases with the increasing of tube row number N, and when $N > 4$, the decreasing trend slows down. When $N > 6$, the variations of

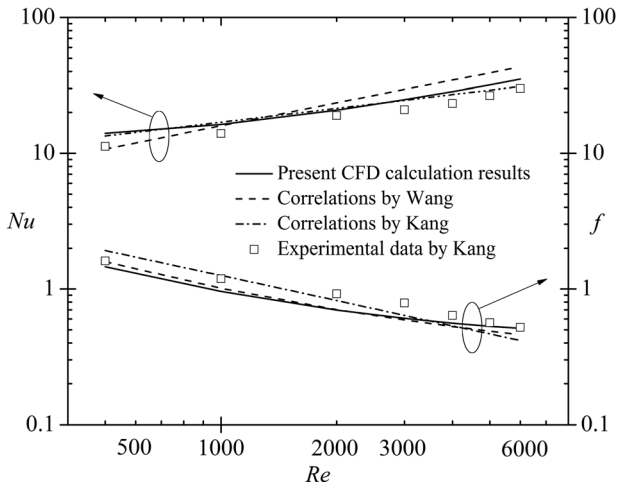

Fig. 5 Comparison between the present CFD results and well-known correlations

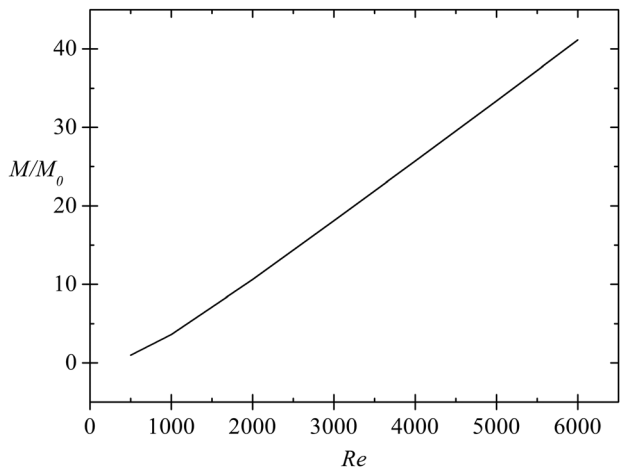

Fig. 6 Variation curve of M/M_0 with Re

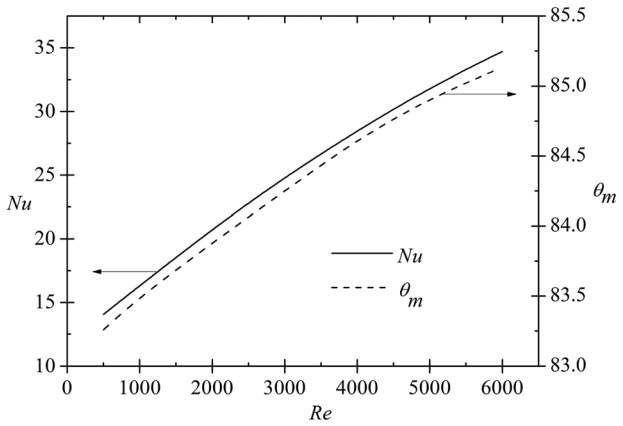

Fig. 7 Comparison between the variation trend of Nu and θ_m with Re

friction factor and Nusselt number are quite subtle, making it reasonable to conclude that the effect of tube row on the heat transfer and fluid flow could be neglected when the number of tube rows is greater than six.

Figure 13 shows the variation of M/M_0 and θ_m with the increasing tube row number, where M_0 is the M value for 1-row case. As can be seen, the average product of $|\vec{U}|$ and $|\text{grad}T|$ decreases with the increasing of N. It also can be found that the intersection angle between air flow velocity and temperature gradient increases with the increasing of tube row number and the increasing trend slows down when $N > 4$. This explains well the change in trend of Nusselt with the increasing of N.

To get a more vivid impression, two more figures, Figs. 14 and 15, together with Fig. 9, comparisons of local distributions of velocity vector, isothermals and intersection angle on the x-y plane for 3-row case, 6-row case, and 9-row case are presented. It is obvious that as the number of tube rows increases, the percentage of the area which has deteriorated synergy (red area) increases. It is also found that when $N > 6$, the flow field, temperature field and the distribution of intersection angle are marked with obvious periodicity, shown by the dashed frame in Fig. 15.

It should be noted that the above discussion is based on values averaged over the whole simulation domain, while to use volume average theory to optimize the heat exchangers, we are more concerned about values averaged over a selected REV. As a result,

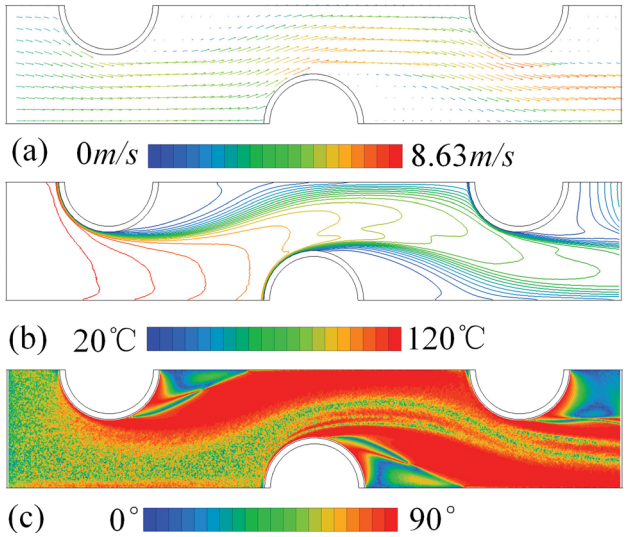

Fig. 9 Re = 3000, $N = 3$, (*a*) velocity, (*b*) temperature, and (*c*) intersection angle

although we arrived at the conclusion that when the number of tube rows is larger than six, the flow field and thermal field could be considered as periodic in the streamwise direction, we cannot say that the computational domain including six tube rows is long enough to get a reasonable lower scale solution. In-depth observations should be carried out on the variation of concerned parameters for every single REV along the air flow direction. Thus, we divided the computational domain of the 7-, 8-, and 9-row cases into 7, 8, and 9 REVs and then calculated the Nusselt numbers, M values and intersection angles for the total 24 elementary volumes, and plotted the variation curves in Fig. 16. Some conclusions that can be drawn from the graphs are the following:

(1) The averaged local M value over every single elementary volume decreases along with the direction of air flow. This is why the magnitude of M averaged over the whole domain decreases as the number of tube rows increase.
(2) Since the curves of M for the three cases collapse to a single curve, it is reasonable to say that the number of tube rows has no effect on the trend of local M from the domain inlet all the way to the outlet.

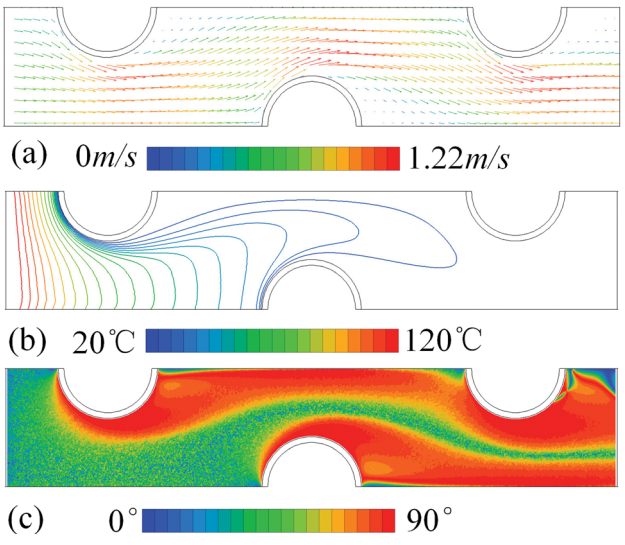

Fig. 8 Re = 500, $N = 3$, (*a*) velocity, (*b*) temperature, and (*c*) intersection angle

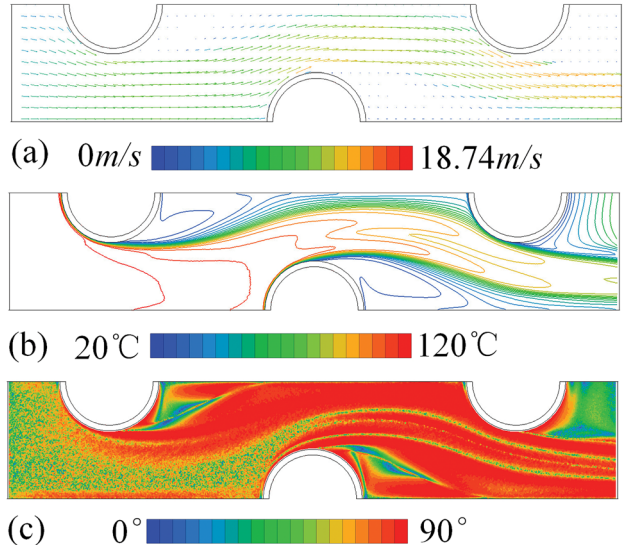

Fig. 10 Re = 6000, $N = 3$, (*a*) velocity, (*b*) temperature, and (*c*) intersection angle

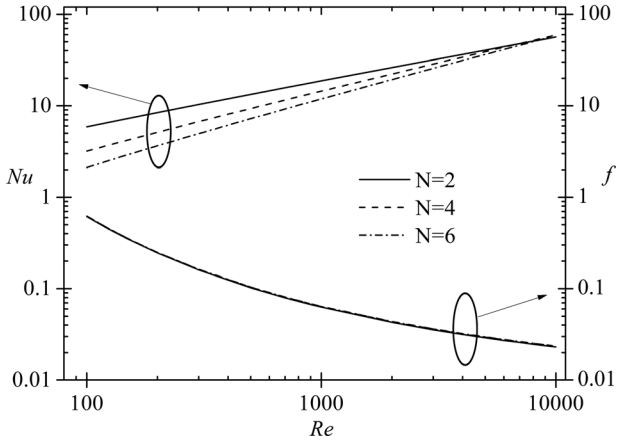

Fig. 11 Effect of tube row number on the heat transfer and friction characteristics, according to Wang correlations [13]

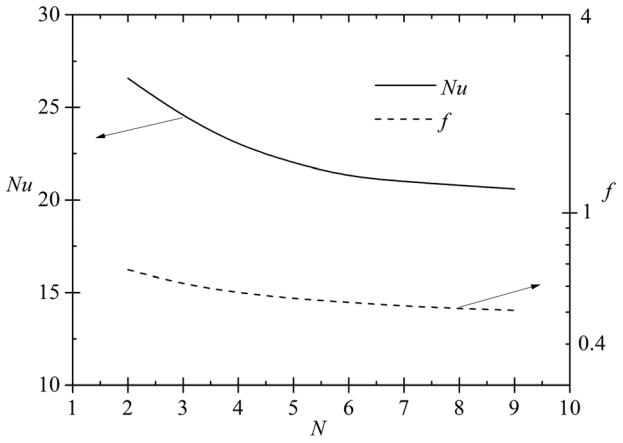

Fig. 12 Variation of Nu and *f* with tube row number by CFD simulation

(3) Excluding the last data point, the curves of Nu and θ_m also collapse to two single curves. However, the Nu number and intersection angle for the last elementary volume is unusual due to the reason that the air-flow recirculation happens when it flows from the trailing edge of the fin to the extended domain. For this reason, the solution of the last volume shouldn't be used to calculate the closure for VAT based model.

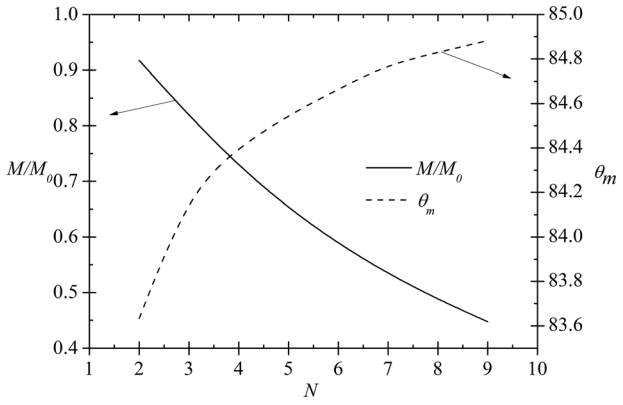

Fig. 13 Variation of *M* and θ_m with tube row number *N*

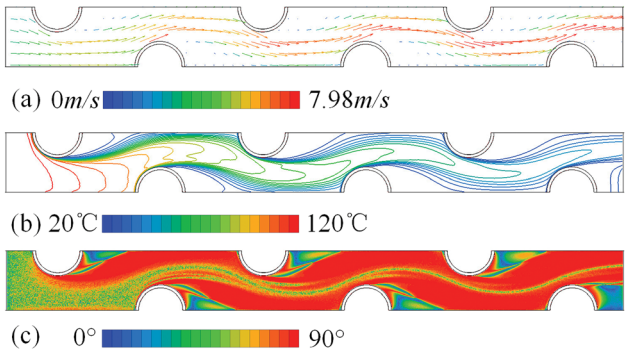

Fig. 14 Re = 3000, *N* = 6, (*a*) velocity, (*b*) temperature, and (*c*) intersection angle

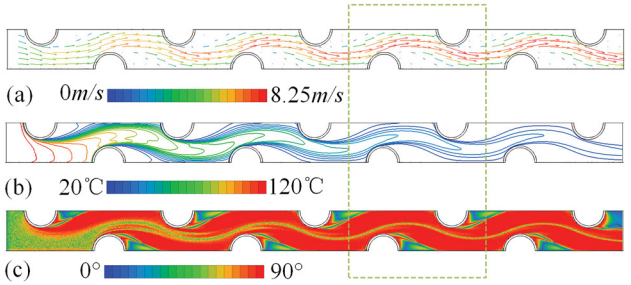

Fig. 15 Re = 3000, *N* = 9, (*a*) velocity, (*b*) temperature, and (*c*) intersection angle

(4) The averaged local Nusselt number decreases along with the direction of air flow and almost keeps constant when $x/P_l > 4$, while the averaged local intersection angle increases along with the direction of air flow and reaches a plateau when $x/P_l > 4$. Both the local averaged Nusselt number and intersection angle for elementary volume five, six, and seven have subtle differences. The variation trends of local averaged Nu and θ_m agree pretty well.

Therefore, in conclusion, $N > 4$ is needed to get a believable local value, which means that the tube row number should not be

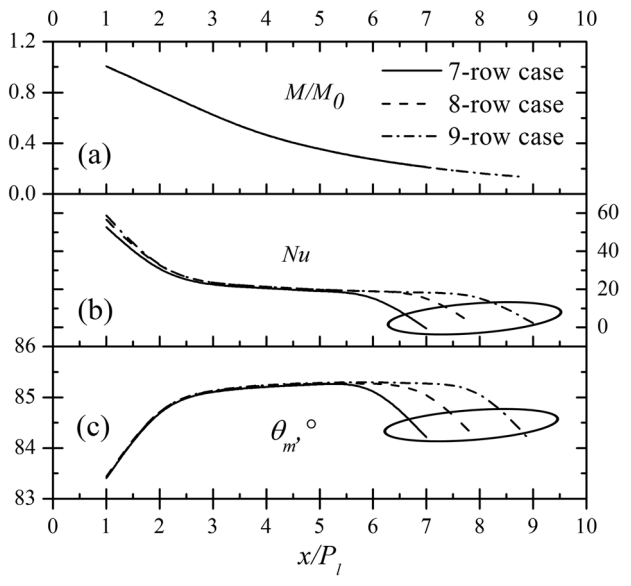

Fig. 16 Variation of local values in the streamwise direction

less than $4+1+1$ rows (the first 4 rows is to develop the velocity and temperature field, and the fifth elementary volume is where to calculate the closure. The solution of the 6th row is not for use considering the invalidity of the last data point). We recommend that $5+2+2$ rows be simulated and that the closure be obtained by averaging the local value over the sixth and seventh elementary volumes.

Concluding Remarks

The present paper describes an effort to determine the tube row number that will be large enough to obtain good estimates of the closure parameters for the VAT-based modeling of fin-and-tube heat exchangers. Simulations were conducted from 1-row to 9-row heat exchangers. The variations of overall Nusselt number and friction factor as well as local values with the increasing of row number were presented. These variation trends were also explained from the view point of the FSP. It was found that when $N>3$, the friction factor could be considered independent of N. As to the Nusselt number, when $N>4$, the variation trend of Nu with N tends to ease up, which agrees well with the increasing trend of intersection angle. When $N>6$, the variations of both local averaged Nusselt number and intersection angle are subtle, and can be regarded as independent of N. For this reason, $4+1+1$ rows of fin-and-tube heat exchanger is the smallest number that will yield a believable local value and a computational domain with $5+2+2$ tube rows is recommended. The present brings us step closer to obtaining closure for the VAT based modeling of fin-and-tube heat exchanger from CFD solutions, which is the subject of future work.

Acknowledgment

The support of a Department of Energy NERI grant, Award Number DE-FC07-07ID14827, is gratefully acknowledged. The numerical calculations were performed using commercial CFD software SC/Tetra Version 8, a product of Software Cradle Co., Ltd.

Nomenclature

A = area, m^2
A_f = fin surface area, m^2
A_o = total surface area, m^2
A_{wp} = the cross flow projected area, m^2
A_w = wetted surface, m^2
c_d = drag coefficient
c_p = specific heat, $J/(kg \cdot K)$
D_o = outer diameter of the tube, m
D_i = inner diameter of the tube, m
D_c = fin collar outside diameter, $D_c = D_o + 2\delta_f$, m
D_h = hydraulic diameter, m
F_p = fin pitch, m
f = Moody friction factor
h = heat transfer coefficient, $W/(m^2 \cdot K)$
k = thermal conductivity, $W/(m \cdot K)$
$m = \sqrt{\frac{2h}{k_f \delta_f}}$, parameter
$\langle m \rangle$ = the average porosity
$\dot{m}$ = mass flow rate, kg/s
n = the number of control volumes
$M = \frac{\sum(|\vec{U}||\nabla T|)}{n}$, parameter
M_0 = the base value of, M
N = the number of tube rows
Nu = Nusselt number
p = pressure, Pa
Δp = pressure drop, Pa
Pr = Prandtl number
P_t = transverse tube pitch, m
P_l = longitudinal tube pitch, m
r = radius of tube, including collar thickness, m
Re = Reynolds number scaled with fin collar outside diameter and maximum velocity, $\mathrm{Re} = \frac{u_{\max} D_c}{\nu}$
R_{eq} = equivalent radius for circular fin, m
S_w = specific surface, 1/m
S_{wp} = the cross flow projected area per volume, 1/m
T = fluid temperature, K
ΔT = logarithmic mean temperature difference, K
T_s = solid temperature, K
u, v, w = x-,y-,z-direction velocity term, m/s
U = velocity vector
X_L = geometric parameter, m

$$\begin{cases} \frac{\sqrt{\left(\frac{P_t}{2}\right)^2 + P_l^2}}{2}, & \text{for staggered layout} \\ \frac{P_l}{2}, & \text{for inline and } 1-\text{row layout} \end{cases}$$

$X_M = P_t/2$, geometric parameter, m

Greek Symbols

δ_f = thickness of a fin, m
η_o = surface efficiency
η_f = fin efficiency
θ = intersection angle, °
μ = viscosity, Pa·s
ν = kinetic viscosity, m^2/s
ρ = density, kg/m^3
τ_{wL} = laminar shear stress, Pa
τ_{wT} = turbulent shear stress, Pa
Φ = heat transfer rate, W
$\Delta\Omega$ = volume of the REV, m^3

Subscripts and Superscripts

$\sim$ = a value in the fluid averaged over the representative volume
$-$ = indicates an average of turbulent values
$\wedge$ = fluctuation of a value
$\langle f \rangle_f$ = means the superficial average of the function, f
f = fin surface or fluid phase
in = air-side inlet
max = maximum value
m = mean value
out = air-side outlet
s = solid phase
T = turbulent
w = tube wall

References

[1] Travkin, V., and Catton, I., 1995, "A Two-Temperature Model for Turbulent Flow and Heat Transfer in a Porous Layer," J. Fluids Eng., **117**(1), pp. 181–188.
[2] Travkin, V. S., and Catton, I., 1998, "Porous Media Transport Descriptions—Non-Local, Linear, and Non-Linear Against Effective Thermal/Fluid Properties," Adv. Colloid Interface Sci., **76–77**, pp. 389–443.
[3] Travkin, V. S., and Catton, I., 2001, "Transport Phenomena in Heterogeneous Media Based on Volume Averaging Theory," *Advances in Heat Transfer*, G. G. Hari, and A. H. Charles, eds., Elsevier, San Diego, CA, pp. 1–144.
[4] Catton, I., 2006, "Transport Phenomena in Heterogeneous Media Based on Volume Averaging Theory," Heat Mass Transfer, **42**(6), pp. 537–551.
[5] Horvat, A., and Catton, I., 2003, "Numerical Technique for Modeling Conjugate Heat Transfer in an Electronic Device Heat Sink," Int. J. Heat Mass Transfer, **46**(12), pp. 2155–2168.
[6] Horvat, A., and Mavko, B., 2005, "Hierarchic Modeling of Heat Transfer Processes in Heat Exchangers," Int. J. Heat Mass Transfer, **48**(2), pp. 361–371.
[7] Whitaker, A., 1999, *The Method of Volume Averaging*, Kluwer Academic Publishers, Boston.
[8] Rich, D. G., 1975, "The Effect of the Number of Tubes Rows on Heat Transfer Performance of Smooth Plate Fin-and-Tube Heat Exchangers," ASHRAE Trans., **81**, pp. 307–317.

[9] McQuiston, F. C., 1978, "Correlations of Heat Mass and Momentum Transport Coefficients for Plate-Fin-Tube Heat Transfer Surfaces With Staggered Tubes," ASHRAE Trans. **84**, pp. 294–308.
[10] Rich, D. G., 1973, "The Effect of Fin Spacing on the Heat Transfer and Friction Performance of Multirow, Smooth Plate Fin-and-Tube Heat Exchangers," ASHRAE Trans., **79**(2), pp. 135–145.
[11] Gray, D. L., and Webb, R. L., "Heat Transfer and Friction Correlations for Plate Fin-and-Tube Heat Exchangers Having Plain Fins," Proceedings Eighth International Heat Transfer Conference, pp. 2745–2750.
[12] Kang, H. J., Li, W., Li, H. Z., Xin, R. C., and Tao, W. Q., 1994, "Experimental Study on Heat Transfer and Pressure Drop Characteristics of Four Types of Plate Fin-and-Tube Heat Exchanger Surfaces," J. Therm. Sci., **3**(1), pp. 34–42.
[13] Wang, C.-C., Chi, K.-Y., and Chang, C.-J., 2000, "Heat Transfer and Friction Characteristics of Plain Fin-and-Tube Heat Exchangers, Part II: Correlation," Int. J. Heat Mass Transfer, **43**(15), pp. 2693–2700.
[14] Torikoshi, K., Xi, G., Nakazama, Y., and Asano, H., 1994, "Flow and Heat Transfer Performance of a Plate Fin-and-Tube Heat Exchanger," ASME J. Heat Transfer, **4**, pp. 411–416.
[15] Jang, J.-Y., Wu, M.-C., and Chang, W.-J., 1996, "Numerical and Experimental Studies of Three Dimensional Plate-Fin and Tube Heat Exchangers," Int. J. Heat Mass Transfer, **39**(14), pp. 3057–3066.
[16] Jang, J.-Y., and Chen, L.-K., 1997, "Numerical Analysis of Heat Transfer and Fluid Flow in a Three-Dimensional Wavy-Fin and Tube Heat Exchanger," Int. J. Heat Mass Transfer, **40**(16), pp. 3981–3990.
[17] Jang, J.-Y., and Yang, J.-Y., 1998, "Experimental and 3-D Numerical Analysis of the Thermal-Hydraulic Characteristics of Elliptic Finned-Tube Heat Exchangers," Heat Transfer Eng., **19**(4), pp. 55–67.
[18] Guo, Z. Y., Li, D. Y., and Wang, B. X., 1998, "A Novel Concept for Convective Heat Transfer Enhancement," Int. J. Heat Mass Transfer, **41**(14), pp. 2221–2225.
[19] Ma, L.-D., Li, Z.-Y., and Tao, W.-Q., 2007, "Experimental Verification of the Field Synergy Principle," Int. Commun. Heat Mass Transfer, **34**(3), pp. 269–276.
[20] Tao, W. Q., He, Y. L., Wang, Q. W., Qu, Z. G., and Song, F. Q., 2002, "A Unified Analysis on Enhancing Single Phase Convective Heat Transfer With Field Synergy Principle," Int. J. Heat Mass Transfer, **45**(24), pp. 4871–4879.
[21] Guo, Z. Y., Tao, W. Q., and Shah, R. K., 2005, "The Field Synergy (Coordination) Principle and Its Applications in Enhancing Single Phase Convective Heat Transfer," Int. J. Heat Mass Transfer, **48**(9), pp. 1797–1807.
[22] He, Y. L., Tao, W. Q., Song, F. Q., and Zhang, W., 2005, "Three-dimensional Numerical Study of Heat Transfer Characteristics of Plain Plate Fin-and-Tube Heat Exchangers From View Point of Field Synergy Principle," Int. J. Heat Fluid Flow, **26**(3), pp. 459–473.
[23] Tao, W. Q., 2001, Numerical Heat Transfer, Xi'an Jiaotong University Press, Xi'an.
[24] Incropera, F. P., DeWitt, D. P., and Ber, T. L., 2006, *Fundamentals of Heat and Mass Transfer*, Wiley, New York.
[25] Cheng, Y. P., Qu, Z. G., Tao, W. Q., and He, Y. L., 2004, "Numerical Design of Efficient Slotted Fin Surface Based on the Field Synergy Principle," Numer. Heat Transfer, Part A, **45**(6), pp. 517–538.
[26] Xie, G., Wang, Q., and Sunden, B., 2009, "Parametric Study and Multiple Correlations on Air-Side Heat Transfer and Friction Characteristics of Fin-and-Tube Heat Exchangers With Large Number of Large-Diameter Tube Rows," Appl. Therm. Eng., **29**(1), pp. 1–16.
[27] Patankar, S. V., 1980, *Numerical Heat Transfer and Fluid Flow*, Hemisphere Publishing Corp., Washington, DC.
[28] Kupprn, T., 2000, *Heat Exchanger Design Handbook*, Marcel Dekker, Inc., New York.
[29] Bejan, A., and Kraus, A., 2003, *Heat Transfer Handbook* Wiley, New York.
[30] Schmidt, T. E., 1949, "Heat Transfer Calculations for Extended Surfaces," Refrig. Eng., **57**, pp. 351–357.
[31] Tao, W.-Q., Guo, Z.-Y., and Wang, B.-X., 2002, "Field Synergy Principle for Enhancing Convective Heat Transfer—Its Extension and Numerical Verifications," Int. J. Heat Mass Transfer, **45**(18), pp. 3849–3856.
[32] Kays, W. M., and Crawford, M. E., 1980, *Convective Heat and Mass Transfer*, McGraw-Hill Book Company, New York.
[33] Wang, C.-C., Chang, Y.-J., Hsieh, Y.-C., and Lin, Y.-T., 1996, "Sensible Heat and Friction Characteristics of Plate Fin-and-Tube Heat Exchangers Having Plane Fins," Int. J. Refrigeration, **19**(4), pp. 223–230.
[34] Wang, C.-C., and Chi, K.-Y., 2000, "Heat Transfer and Friction Characteristics of Plain Fin-and-Tube Heat Exchangers, Part I: New Experimental Data," Int. J. Heat Mass Transfer, **43**(15), pp. 2681–2691.